Published as: *Science*. 2014 April 18; 344(6181): 307–310.

The structural basis of pathogenic subgenomic flavivirus RNA (sfRNA) production

Erich G. Chapman[1,2], **David A. Costantino**[1,2], **Jennifer L. Rabe**[1], **Stephanie L. Moon**[3], **Jeffrey Wilusz**[3], **Jay C. Nix**[4], and **Jeffrey S. Kieft**[1,2,*]

[1]Department of Biochemistry and Molecular Genetics University of Colorado Denver School of Medicine, Aurora, Colorado, 80045, USA

[2]Howard Hughes Medical Institute, University of Colorado Denver School of Medicine, Aurora, Colorado, 80045, USA

[3]Department of Microbiology, Immunology and Pathology, Colorado State University, Fort Collins, Colorado, 80523, USA

[4]Molecular Biology Consortium, Advanced Light Source, Lawrence Berkeley National Laboratory, Berkeley, California, 94720, USA

Abstract

Flaviviruses are emerging human pathogens and worldwide health threats. During infection, a pathogenic, subgenomic flaviviral RNAs (sfRNAs) are produced by resisting degradation by the 5'→3' host cell exonuclease Xrn1 through an unknown RNA structure-based mechanism. Here, we present the crystal structure of a complete Xrn1-resistant flaviviral RNA, which contains interwoven pseudoknots within a compact structure that depends on highly-conserved nucleotides. The RNA's three-dimensional topology creates a ring-like conformation with the 5' end of the resistant structure passing through the ring from one side of the fold to the other. Disruption of this structure prevents formation of sfRNA during flaviviral infection. Thus, sfRNA formation results from an RNA fold that interacts directly with Xrn1, presenting the enzyme with a structure that confounds its helicase activity.

Flaviviruses (FVs, including Dengue, West Nile, Yellow Fever, Japanese Encephalitis, and others) are single-stranded positive-sense RNA viruses and emerging worldwide human health threats (1–3). During infection by arthropod-borne FVs not only is the viral genomic RNA (gRNA) replicated, but specific 300–500 nucleotide-long subgenomic flaviviral RNAs (sfRNAs) also accumulate (4–9). These sfRNAs relate directly to disease, being essential for FV pathogenicity in fetal mice and for cytopathicity in cultured cells (5), through several proposed mechanisms (10–13). sfRNAs are produced through incomplete degradation of viral gRNA by the 5'→3' host-cell exonuclease Xrn1 (14), which halts at defined locations

*Correspondence to: Jeffrey.Kieft@ucdenver.edu.

Supplementary Materials
Materials and Methods
Figs. S1 to S9
Table S1
References (1–3, 5–11)

within the gRNA's 3' untranslated region (3'UTR), forming sfRNAs (fig. S1A) (5). Biochemical studies suggest that an independently folded RNA structures are responsible for this programmed Xrn1 resistance (15–17); however, the structure-based mechanism remains unknown.

Xrn1 resistance is conferred by discrete RNA sequences conserved across FVs that we refer to as Xrn1-resistant RNAs (xrRNAs) (15). Alignment of putative xrRNA sequences (fig. S1B) suggests a shared structure that includes a three-way junction surrounded by conserved nucleotides and the potential to form a pseudoknot (Fig. 1A) (5, 16, 17). To identify xrRNAs suitable for structural studies, we used a previously validated assay using purified Xrn1 from *K. lactis* to test the Xrn1 resistance of putative xrRNAs from different arthropod-borne FVs (15); all were resistant *in vitro* (fig. S1C). The sequence alignments and functional data suggest that the structure of any one FV xrRNA is representative of all, therefore we determined the structure of a functional xrRNA from Murray Valley Encephalitis (MVE) Virus (Fig. 1B,C) to 2.5 Å resolution using X-ray crystallography (fig. S2). The RNA adopts a compact structure with helices P1 and P2 stacked coaxially and helix P3 at an acute angle relative to P1 (Fig. 1D), consistent with other RNA three-way junctions of this class (fig. S3) (18). Helices P1 and P3 form a ring-like structure defined by nucleotides 33–49, which comprise a continuous loop that resides entirely on one side of the structure. The 5'end of the xrRNA passes directly through the center of the ring, crossing from one side of the structure to the other (fig. S4). The ring-like side of the xrRNA that Xrn1 encounters as it approaches in a 5'→3' direction (the 'front') is concave, with the phosphate backbone defining the rim of the concavity, the major groove the inner surface, and the RNA that the enzyme must pull into the active site emerging from the center (Fig. 1D). In the crystal structure the putative RNA pseudoknot is not formed but the relevant bases are in a conformation where they can readily pair; this would allow the P4-L4 hairpin to stack under helix P3. The structure shows that the pseudoknot is not essential for folding of the three-way junction, formation of the ring, or placement of the 5' end through the ring, however it does enhance resistance (fig S5A,B). Stem-loop P4-L4 does not interact with the rest of the xrRNA and can be removed without compromising Xrn1-resistance (fig. S5C) (15). Upon encountering the xrRNA, Xrn1 must pull the 5' end of the RNA through the ring. Rather than simply unwinding a prototyptical RNA helix, unfolding this xrRNA requires that Xrn1 essentially turn the structure inside-out (Fig 2A). In contrast, the virally encoded RNA-dependent RNA polymerase approaching from the 3' end during (−) strand synthesis would not encounter this impediment, suggesting the three-dimensional topology confers the characteristic of unidirectional resistance.

The three-helix junction is the core of the xrRNA structure but is not independently folded; its structure depends on interactions with the 5' end (Fig. 2B, and fig S7A–C). Specifically, C5 base-pairs with G46, and this pair stacks on a platform formed by intrastrand pairing of U47 with the Hoogsteen face of A49 (. 2B). This stacking diverts the RNA chain to the space between P1 and P3 where U4 makes a base triple in the major groove of the A24-U38 pair; all three of these nucleotides are absolutely conserved. This interaction holds P1 and P3 together in a conformation further stabilized by inner-sphere coordination of a magnesium ion by the phosphates of C5 and A6 (fig. S7D). The next-most 5' nucleotide, G3, forms a

Watson-Crick (WC) base pair with junction nucleotide C40. Disruption of this base pair by mutation of either base (G3C and C40G) abolished the ability of the MVE RNA to resist Xrn1 degradation (Fig. 2C). The double mutant (G3C+C40G), designed to restore the base pairing, did not restore resistance. This is likely due to the formation of incorrect but stable structure induced by mutation, precluding restoration of proper base-pairing interactions in the double mutant (*i.e.* the C40G mutant could form a C–G pair with C22 that G3C cannot compete with). An additional intramolecular interaction involves U2, which was mutated to a G in the crystallized RNA. Nucleotide A41 in the three-way junction is poised to form a Watson-Crick pair with U2 in the WT sequence, and there is covariation between these positions (fig. S1B, D). Together, this suggests the U2-A41 pair naturally forms; however the structure folds and resists Xrn1 even when it is not present. The only nucleotide in the three-way junction that does not make base pair interactions with the 5’ end of the RNA is C22, which makes hydrogen bonds with U43, C44, and perhaps U45 through phosphates, nucleobase functional groups, and C22’s 2’-hydroxyl (fig. S7E). Mutation of conserved C22 (C22G) eliminates Xrn1 resistance *in vitro* by the crystallized MVE RNA (Fig. 2C), by xrRNAs from Dengue and from the Kunjin strain of West Nile Virus (WNV_{KUN}; a proven model for FV infection), and also disrupts sfRNA production during WNV_{KUN} infection (15).

The U2-A41 and G3-C40 base pairs comprise a second, previously unidentified pseudoknot in the xrRNA structure between S1 and S3 that is interwoven with the S4-L3 pseudoknot (fig. S8). Within the structure, these pseudoknot interactions couple the junction conformation with positioning of the 5’ end of the xrRNA through the P1/P3 ring. To test the importance of these structural features during infection, we disrupted the three 5’-most nucleotides in two xrRNA structures in WNV_{KUN} (Fig 3A, S6B) and monitored sfRNA production during infection in human cells by these viruses. WT virus produces multiple sfRNAs; the two largest, sfRNA1 and sfRNA2, are produced by Xrn resistance of xrRNA1 and xrRNA2, respectively (Fig. 3B). Mutation of xrRNA1 (mut xrRNA1, fig. S6B) eliminated sfRNA1 production, mutation of xrRNA2 (mut xrRNA2, fig. S6B) eliminated sfRNA2 production (mut xrRNA2 also decreased sfRNA1 production as has been reported previously (15)), and a double mutant (mut xrRNA1+2, fig. S6B) eliminated both sfRNA1 and 2, indicating the 5’ end-junction interaction is essential for sfRNA formation during infection. The P1/P3 ring is closed on the side opposite the junction by extrusion and stacking of A33 upon the U47-A49 platform at the base of P1 (Fig. 2B). Although folding of the 5’ end with the junction is sufficient to form the ring, we propose that closing of the S4-L3 pseudoknot provides the final ‘latch’ that fully stabilizes the conformation (fig. S5A). Consistent with this, chemical probing suggests the S4-L3 pseudoknot is conformationally dynamic or transiently formed and the structure of the three-way junction, the 5’ end, and the pseudoknot are coupled (15).

We mapped the 5’ terminus of the RNA product resulting from resistance to a point two nucleotides upstream of the 5’ end of the RNA we crystallized (fig. S9A), consistent with studies of other xrRNAs (4, 5, 15, 17). Using the structure of Xrn1 from *D. melanogaster* bound to a substrate analog (19), we modeled the xrRNA structure in position with the last nucleotide to be processed in the Xrn1 active site (Fig. 3C,D, and fig. S9B–D). When the

enzyme halts, the xrRNA directly contacts Xrn1's surface, positioned in a cleft, with its ring structure braced over the entry to the active site and conserved nucleotides in position to contact the protein (fig. S1D). The Xrn1-xrRNA contacts may further stabilize the xrRNA fold or prevent conformational changes hypothesized to be important for helicase activity. It is proposed that Xrn1's helicase activity is conferred by Brownian motion and the enzyme's 'tower helix' and 'helix α', which interact and unwind with the leading edge of an RNA duplex as it is pulled into the cleft over the active site (19). The model shows that the xrRNA structure is braced against the enzyme, holding the leading edge of the relevant RNA duplex behind the concave ring structure and away from these helices, suggesting a mechanism for RNA structure-driven Xrn1 and by extension sfRNA production.

Supplementary Material

Refer to Web version on PubMed Central for supplementary material.

Acknowledgments

We thank the members of the Kieft Lab for discussions, and A. Ferré-d'Amaré, M. Johnston, and R. Batey for critical reading of this manuscript. The UC Denver X-ray Facility is supported by UC Cancer Center Support Grant P30CA046934. J.S.K. is an Early Career Scientist of the Howard Hughes Medical Institute. J.W. was supported by an NIH award through the Rocky Mountain Regional Center of Excellence, U54 AI-065357. Coordinates and structure factors have been deposited with PDB accession code 4PQV.

References and Notes

1. Bhatt S, et al. Nature. 2013; 496:504–507. [PubMed: 23563266]
2. Mackenzie JS, Gubler DJ, Petersen LR. Nat Med. 2004; 10:S98–S109. [PubMed: 15577938]
3. Normile D. Science. 2013; 342:415. [PubMed: 24159024]
4. Lin KC, Chang HL, Chang RY. J. Virol. 2004; 78:5133–5138. [PubMed: 15113895]
5. Pijlman GP, et al. Cell Host Microbe. 2008; 4:579–591. [PubMed: 19064258]
6. Wengler G, Gross HJ. Virology. 1978; 89:423–437. [PubMed: 568848]
7. Naeve CW, Trent DW. J. Virol. 1978; 25:535–545. [PubMed: 625082]
8. Takeda H, Oya A, Hashimoto K, Yasuda T, Yamada MA. J. Gen. Virol. 1978; 38:281–291. [PubMed: 564392]
9. Urosevic N, van Maanen M, Mansfield JP, Mackenzie JS, Shellam GR. J. Gen. Virol. 1997; 78(Pt 1):23–29. [PubMed: 9010281]
10. Schuessler A, et al. J. Virol. 2012; 86:5708–5718. [PubMed: 22379089]
11. Moon SL, et al. RNA. 2012; 18:2029–2040. [PubMed: 23006624]
12. Schnettler E, et al. J. Virol. 2012; 86:13486–13500. [PubMed: 23035235]
13. Roby JA, Pijlman GP, Wilusz J, Khromykh AA. Viruses. 2014; 6:404–427. [PubMed: 24473339]
14. Jones CI, Zabolotskaya MV, Newbury SF. Wiley Interdiscip. Rev. RNA. 2012; 3:455–468. [PubMed: 22383165]
15. Chapman EG, Moon SL, Wilusz J, Kieft JS. eLife. 2014 **in press**.
16. Funk A, et al. J. Virol. 2010; 84:11407–11417. [PubMed: 20719943]
17. Silva PA, Pereira CF, Dalebout TJ, Spaan WJ, Bredenbeek PJ. J. Virol. 2010; 84:11395–11406. [PubMed: 20739539]
18. Lescoute A, Westhof E. RNA. 2006; 12:83–93. [PubMed: 16373494]
19. Jinek M, Coyle SM, Doudna JA. Mol. Cell. 2011; 41:600–608. [PubMed: 21362555]

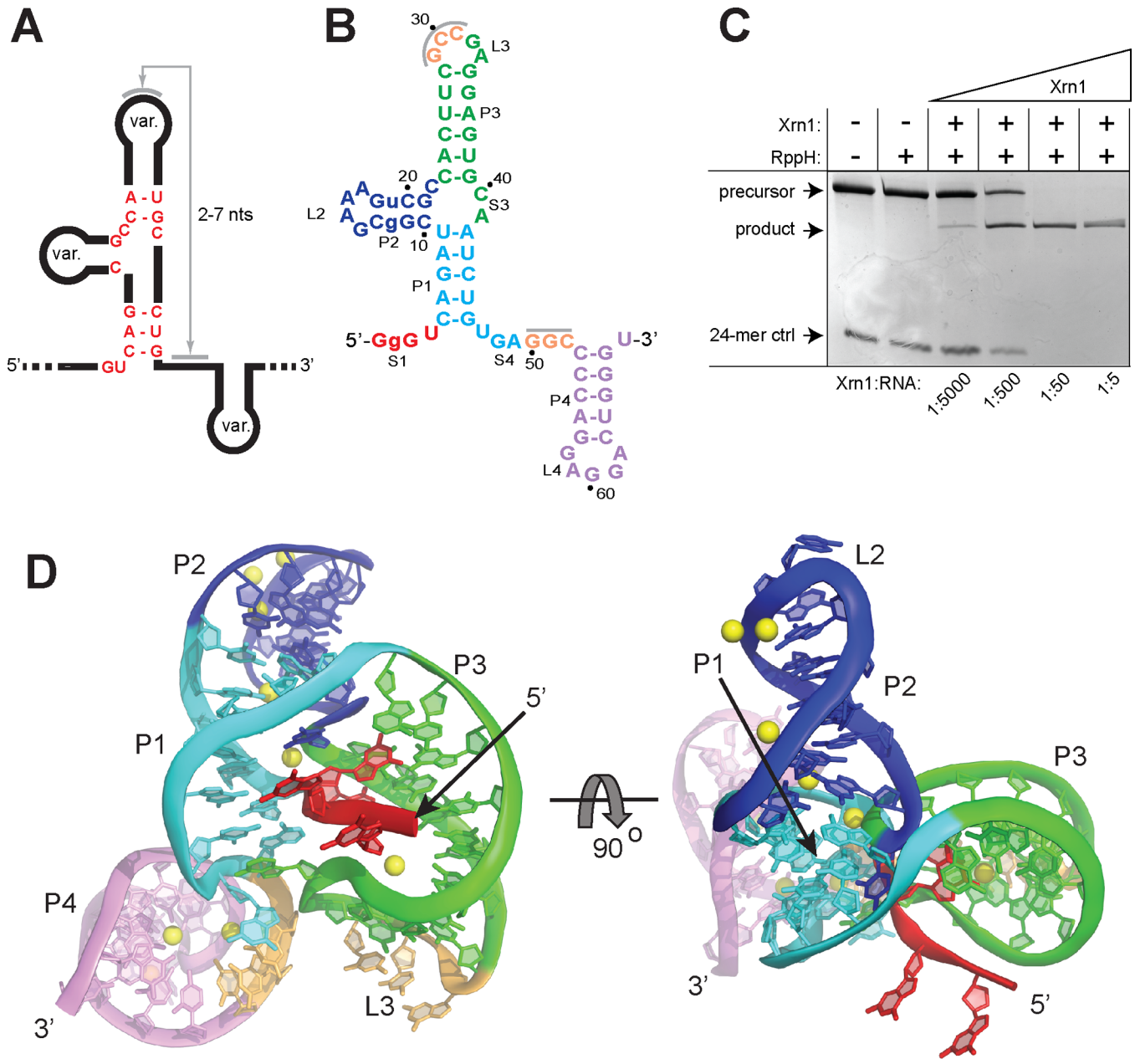

Fig. 1.

Crystal structure of an xrRNA. **(A)** Conserved secondary structure and sequence (red) of xrRNAs. Var. indicates elements of variable size and sequence. **(B)** Crystallized RNA sequence from MVE. Lower-case nucleotides were altered from WT. The U2G mutation was made to increase transcription yields, but neither this nor the other mutation affected function (panel C). Grey bars indicate a putative pseudoknot interaction. **(C)** Gel demonstrating Xrn1 resistance by the crystallized RNA, using an assay with Xrn1 from *K. lactis* that was validated in a previous publication (15). The precursor is the crystallized RNA with a 30-nt 5' leader. A 24-mer monophosphorylated RNA was included as a control for Xrn1 activity. Under these conditions, each Xrn1 molecule processes multiple copies of the xrRNA, and there is no in-trans protection of the 24-mer. This does not preclude a role

for sfRNA as a transient Xrn1 inhibitor during infection (11, 15). **(D)** Two views of the structure, colored to match figure 1D. Yellow: Mg^{2+} ions.

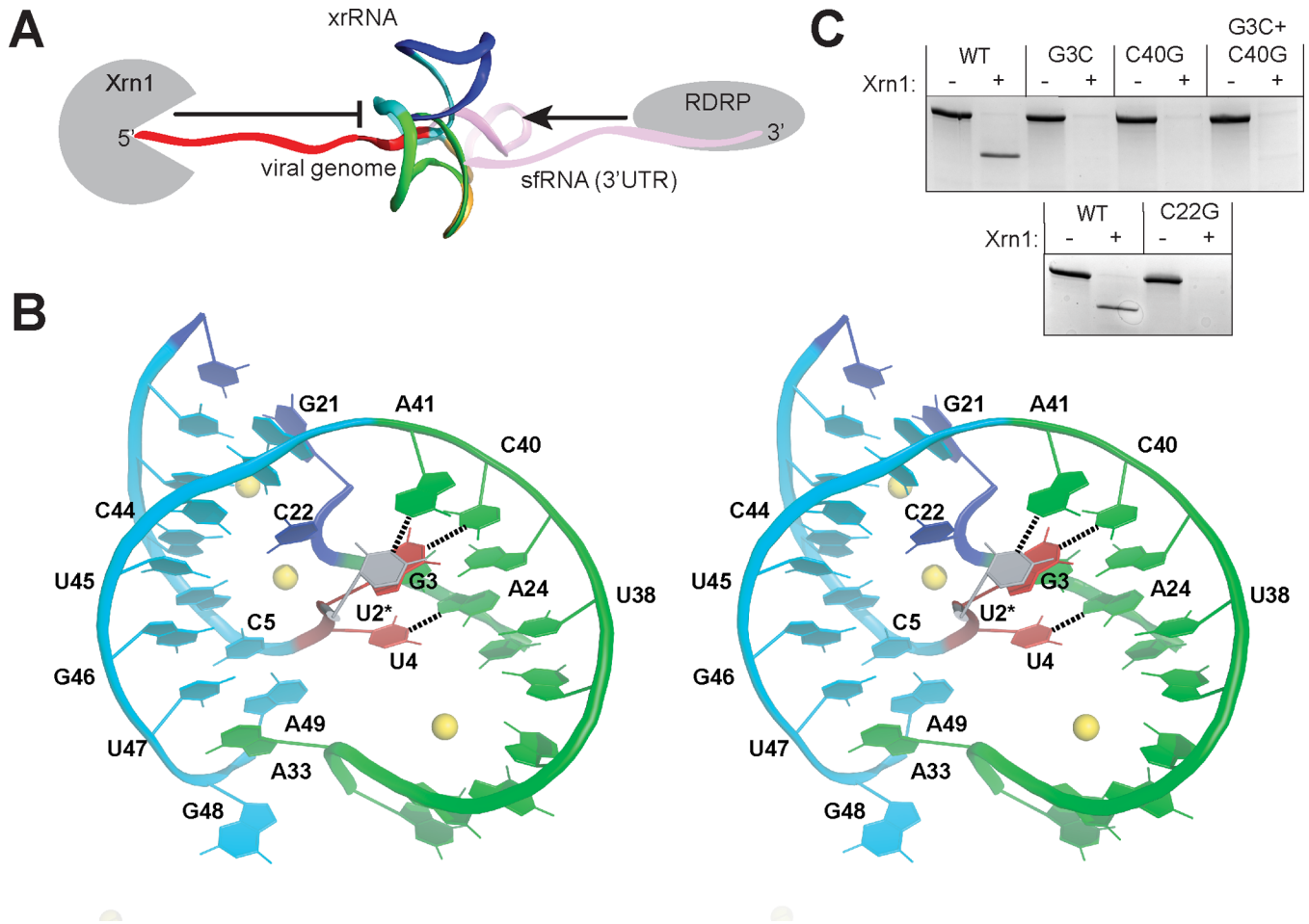

Fig. 2.

Formation and importance of the junction and ring structures **(A)** Structure (backbone ribbon) placed in context with upstream and downstream RNA and enzymes that approach from each side (not to scale). **(B)** Stereo view of the P1–P3 ring and 5' end of the xrRNA, colored to match figure 1D and 2A. U2, which was mutated to a G, is shown modeled in position in grey. Base pairs between the 5' nucleotides and P3 are shown with dashed lines. **(C)** Xrn1 resistance assays of mutant RNAs based on these interactions (mutant sequences in fig. S6A).

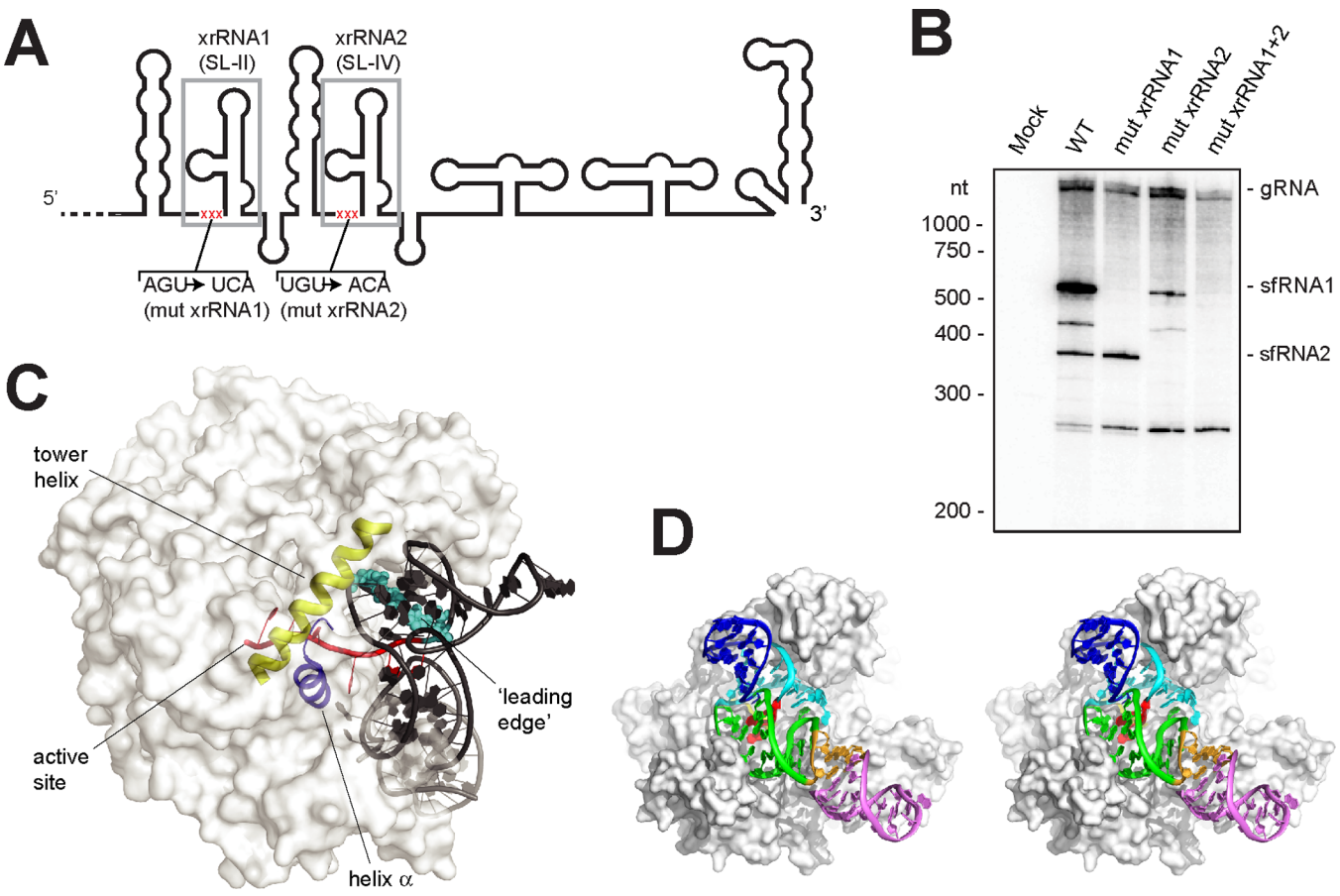

Fig. 3.

Importance of the structure during infection and proposed mechanism of resistance. **(A)** Secondary structure cartoon of the 3'UTR from WNV_{KUN}. Two xrRNAs are boxed in grey and the location of mutations is shown in red. **(B)** Northern blot analysis of total RNA isolated from human cells infected with WT and mutant WNV_{KUN} (mutant sequences in fig. S6B). The location of molecular weight markers and the identity of sfRNA species are indicated to the left and right of the blot respectively. **(C)** Model xrRNA structure on *D. melanogaster* Xrn1 (white surface) (fig. S9). The tower helix (yellow) and helix α (blue) involved in helicase activity, the active site, the RNA entering the active site (red) and leading edge of the helix to be unwound (cyan) are shown. (D) Stereo view of model showing how the xrRNA fits in a cleft in Xrn1's surface.